Effects of Radial Envelope Modulations on the Collisionless Trapped-electron Mode in Tokamak Plasmas

Hao-Tian Chen[1,*] and Liu Chen[1,2,†]

[1] *Institute for Fusion Theory and Simulation and Department of Physics, Zhejiang University, Hangzhou, 310027, People's Republic of China*

[2] *Department of Physics and Astronomy, University of California, Irvine, California 92697, USA*

(Dated: November 10, 2017)

Adopting the ballooning-mode representation and including the effects of radial envelope modulations, we have derived the corresponding linear eigenmode equation for the collisionless trapped-electron mode (CTEM) in tokamak plasmas. Numerical solutions of the eigenmode equation indicate that finite radial envelope modulations can affect the linear stability properties both quantitatively and qualitatively via the significant modifications in the corresponding eigenmode structures.

PACS numbers: 52.30.Gz, 52.35.Kt, 52.35.Qz, 52.55.Fa

I. INTRODUCTION

Micro-turbulence driven by drift-wave instabilities is considered to play important roles in the anomalous transport of tokamak plasmas [1]. Two of the most prevailing drift-wave instabilities in the tokamak core region are generally believed to be the ion temperature gradient (ITG) mode and the collisionless trapped-electron mode (CTEM). Although known for decades of years [1, 2], the linear and nonlinear properties of these modes are still being actively investigated both theoretically and experimentally. Specifically, the effect of finite radial envelope modulation, i.e., finite $\theta_k = i(nq')^{-1}\partial_r \ln A$, on ITG modes has recently received a renewed interest in fusion research [3, 4]. Here, n, q' and A are, respectively, the toroidal mode number, the radial derivative of safety factor q and the radial envelope. It is found that, depending on specific parameters, the most unstable ITG modes can have a finite θ_k and poloidally balloon at the top or bottom of tokamaks. On the other hand, although it has been generally anticipated that the CTEMs are most unstable at $\theta_k = 0$ [5–10], there is, to our knowledge, no rigorous investigation to confirm this anticipation. The main purpose of this paper is, thus, to carefully examine the effect of finite θ_k on the linear stability properties of CTEMs. Such a fundamental study is important because both the finite radial envelope modulation and the linear stability properties play significant roles in the nonlinear dynamics of CTEMs. Our results indicate that finite θ_k can modify the CTEM linear stabilities both quantitatively and qualitatively via significantly altering the corresponding eigenmode structures.

The theoretical model and the corresponding CTEM eigenmode equation are presented in Sec.II. Sec.III contains the numerical results, demonstrating the finite θ_k effects on the linear stabilities and eigenmode structures. Summary and discussions are given in Sec.IV.

*Email: haotianchen@zju.edu.cn

†Email (Corresponding author):liuchen@zju.edu.cn

II. THEORETICAL MODEL

We consider the electrostatic collisionless trapped-electron modes in an axisymmetric, low-β ($\beta = 8\pi P/B^2$), large aspect-ratio ($a/R_0 \ll 1$) tokamak with concentric circular magnetic surfaces, and we use the usual minor radius (r), poloidal angle (θ), and toroidal angle (ζ) coordinates. The equilibrium magnetic field is given by $\vec{B} = B_0[(1-\epsilon\cos\theta)\hat{e}_\zeta + \epsilon/q\hat{e}_\theta]$, with $\epsilon = r/R_0 \ll 1$ and R_0 the major radius. The particle equilibrium distribution function is taken to be local Maxwellian, $F_{0,j} = n_0(\pi v_{tj}^2)^{-3/2}e^{-v^2}$, with $v = V/v_{tj}$, $v_{tj} = \sqrt{2T_j/m_j}$ and $j = i, e$ denoting the particle species. Meanwhile, we adopt the well-known ballooning representation [11, 12] for the fluctuations, e.g., for the perturbed electrostatic potential:

$$\begin{aligned}\delta\phi_n &= e^{-i\omega t - in\zeta}\sum_m e^{im\theta} \\ &\quad\times\int_{-\infty}^{+\infty}\int_{-\infty}^{+\infty} d\eta d\theta_k e^{i(nq-m)\eta - i\theta_k nq}\tilde{\Phi}(\eta,\theta_k).\end{aligned} \tag{1}$$

In Eq. (1), in contrast to the previous investigations [2, 5–7], the present representation contains the finite θ_k effect. Assuming the usual drift ordering $\omega_{te} > \omega_{be} \gg \omega \gg \omega_{ti}, \omega_{di}$ and following standard procedures [2, 7], the eigenmode equation can be derived straightforwardly as

$$\begin{aligned}&[D_1\partial_\eta^2 + (\partial_\eta D_1)\partial_\eta + Q(\eta,\theta_k)]\tilde{\Phi}(\eta) \\ &= \sqrt{\frac{\epsilon}{2}}\int_{\sin^2\frac{\eta}{2}}^1 \frac{d\kappa^2}{K(\kappa)\sqrt{\kappa^2-\sin^2\frac{\eta}{2}}}\frac{\Omega^3[(\Omega-1)T_1+\eta_e T_2]}{\epsilon_n H\Omega_t^2} \\ &\quad\times\sum_{j=-\infty}^{+\infty}\int_{2j\pi-\pi}^{2j\pi+\pi}\delta(\eta-\eta')d\eta'\int_{2j\pi-\eta_0}^{2j\pi+\eta_0}\frac{\tilde{\Phi}(\alpha)d\alpha}{\sqrt{\kappa^2-\sin^2\frac{\alpha}{2}}},\end{aligned} \tag{2}$$

with

$$Q = \frac{2\Omega^2}{\Omega_t^2}\{\Omega(1+\tau) - D_1 + \eta_i\Gamma_0 + \frac{\Omega_t^2}{4\Omega^2}(\partial_\eta^2 D_1 + D_3) + \frac{\epsilon_n D_2}{\tau\Omega}[s(\eta-\theta_k)\sin\eta + \cos\eta]\},$$

$$D_1 = (\tau\Omega+1)\Gamma_0 + \eta_i[b_i\Gamma_1 - (b_i-1)\Gamma_0],$$

$$D_2 = (\tau\Omega+1)[2\Gamma_0 + b_i(\Gamma_1-\Gamma_0)] + \eta_i[2(b_i-1)^2\Gamma_0 + (3-2b_i)b_i\Gamma_1],$$

$$D_3 = k_\theta^4\rho_i^4 s^4(\eta-\theta_k)^2\{(\tau\Omega+1)(\Gamma_0-\Gamma_1) + \eta_i[(3-2b_i)\Gamma_0 + 2(b_i-1)\Gamma_1]\},$$

$$T_1 = \begin{cases} -[1+\sqrt{\frac{\Omega}{\epsilon_n H}}Z(\sqrt{\frac{\Omega}{\epsilon_n H}})] & \text{if } H \geq 0, \\ -[1+i\sqrt{\frac{\Omega}{\epsilon_n |H|}}Z(i\sqrt{\frac{\Omega}{\epsilon_n |H|}})] & \text{if } H < 0, \end{cases}$$

$$T_2 = T_1(\frac{3}{2} - \frac{\Omega}{\epsilon_n H}) + \frac{1}{2}.$$

Eq. (2) corresponds to the quasi-neutrality condition. In deriving Eq. (2), ions are approximated as a fluid but keeping the finite ion Larmor-radius corrections, and circulating electrons are taken to be adiabatic. The right hand side of Eq. (2) contains the bounce-averaged trapped-electron response. Note also that Eq. (2) has the symmetry properties $\tilde{\Phi}(-\eta|-\theta_k) = \pm\tilde{\Phi}(\eta|\theta_k)$ and $\Omega(-\theta_k) = \Omega(\theta_k)$. Thus, the eigenvalue has an extreme point at $\theta_k = 0$. The physical parameters are standardly defined: $\tau = T_e/T_i$, $2b_i = k_\theta^2\rho_i^2[s^2(\eta-\theta_k)^2+1]$, $k_\theta = nq_0/r_0$, r_0 is the reference mode-rational surface, ρ_i is the ion gyroradius, and $s = rq'/q$ at r_0 is the magnetic shear. Meanwhile, $\epsilon_n = r_n/R_0$ with $r_n = |\nabla n_0/n_0|^{-1}$ is the density scale length, and $\eta_{i,e} = d\ln T_{i,e}/d\ln n_0$. The frequencies have been normalized by the electron diamagnetic drift frequency $\omega_{*e} = k_\theta cT_e/(eB_0r_n)$, that is, $\Omega = \omega/\omega_{*e}$, $\Omega_t = 2\epsilon_n/(\tau q k_\theta \rho_i)$. $\Gamma_n = I_n(b_i)\mathrm{Exp}(-b_i)$ with I_n being the modified Bessel function. In the trapped-electron term, $\eta_0 = 2\arcsin\kappa$ is the turning point of a given trapped-electron. $H = 4\hat{s}[E(\kappa)/K(\kappa)+\kappa^2-1]+[2E(\kappa)/K(\kappa)-1]$ is associated with the trapped-electron's precessional frequency, with $K(\kappa)(E(\kappa))$ designating the complete elliptic integral of first (second) kind. Z is the plasma dispersion function, and the branch cut of the square-root function in T_1 is chosen to be the nonpositive imaginary axis.

With the outgoing-wave boundary condition [13], Eq. (2) determines the linear stability properties of CTEMs in toroidal plasmas. As reported in [14, 15], owing to the non-uniformity of the toroidal field over a magnetic surface, there exist two branches of the electron drift eigenmodes in toroidal plasmas: one is slab-like and the other is toroidicity-induced. The slab-like modes are fast oscillating unbounded states along the field line, and experience finite magnetic shear damping effect. Since the fast variation will be averaged out by the bounce motion, the slab-like modes are, typically, CTEM stable. The toroidicity-induced modes, on the other hand, are characterized by quasi-bounded states with exponentially small shear damping through tunnelling leakages. Thus, the toroidicity-induced modes are expected to be destabilized by trapped-electron collisionless or collisional dissipations [7]. The quasi-bounded toroidicity-induced eigenmode structures can be further classified according to their eigenmode number l, i.e., the number of nodes along the field line. The eigenmodes with large eigenmode numbers will not be significantly destabilized by the trapped-electrons due to, again, their fast variation along η. Therefore, only the low-l toroidicity-induced eigenmodes are relevant to the trapped-electron instabilities.

III. NUMERICAL RESULTS

To study the finite θ_k effect, we numerically solve the integro-differential eigenmode equation by using a new eigen-solver [16], which can locate all of the eigenvalues in a closed complex domain. For the $\theta_k = 0$ case, the toroidicity-induced modes possess even and odd parities. While the even modes can be efficiently destabilized by the trapped-electrons, the odd modes are stable, because the trapped electrons bounce average out the fluctuations. Depending on the parameters, the even toroidicity-induced modes can be further categorized into two types [14]: the strong toroidicity-induced modes peaking around $\eta = 0$, and the weak toroidicity-induced modes peaking away from $\eta = 0$.

Figure 1 plots the dependence of the eigenfrequency , $\Omega = \Omega_r + i\Omega_i$, on θ_k for the even- and odd-parity eigenmodes. The parameters are given in the caption. The corresponding eigemode structures for four different values of θ_k, meanwhile, are given in Figs. 2 and 3 for the even- and odd-parity eigenmodes, respectively. Note that the parity is referred to the limit of $\theta_k = 0$. Figure 2 shows that the $\theta_k = 0$ even mode is peaked at $\eta = 0$, confirming it being a strong toroidicity-induced eigenmode. Figure 1 demonstrates that the finite θ_k has indeed a stabilizing effect on the even-parity strong toroidicity-induced mode, consistent with previous studies [5–10]. The odd mode, however, is destabilized by the finite θ_k and the growth rate Ω_i increases with θ_k, until it eventually becomes the dominant instability. Figure 2 explains why the even-parity mode is stabilized by the finite θ_k. Note that at $\theta_k = 0$ the eigenmode structure peaks at $\eta = 0$ and, thus, taps the maximum of the trapped-electron instability drive. As θ_k increases, however, the eigenmode begins to peak away from $\eta = 0$, and, correspondingly, taps less trapped-electron instability drive. Therefore, the even-parity strong toroidicity-induced mode experiences finite θ_k stabilization.

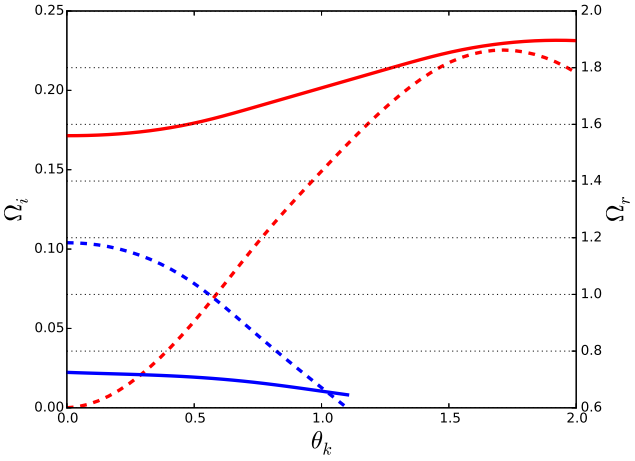

FIG. 1: (Color online) Plots of the eigenfrequencies versus θ_k for the even (blue) and odd (red) parity strong toroidicity-induced eigenmodes. The parameters are $\tau = s = \eta_i = 1$, $q = 1.5$, $\epsilon = 0.2$, $\epsilon_n = 0.4$, $k_\theta \rho_i = 0.2$, $\eta_e = 2$. Solid (dashed) lines are the real frequencies (growth rates).

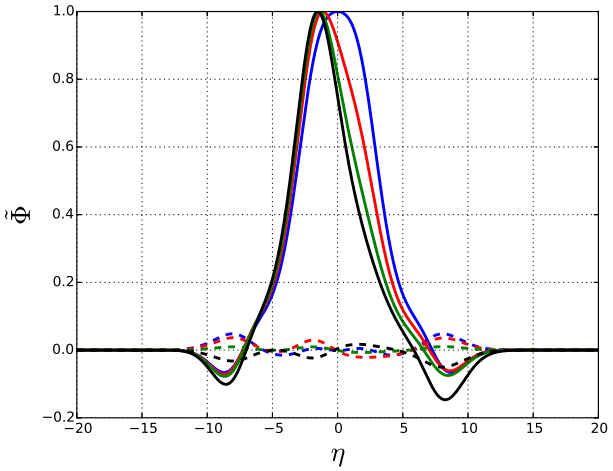

FIG. 2: (Color online) Plots of eigenmode structures of the even-parity strong toroidicity-induced modes for $\theta_k = 0$ (blue), $\theta_k = 0.5$ (red), $\theta_k = 1.0$ (green) and $\theta_k = 1.63$ (black). The solid (dashed) lines correspond to the real (imaginary) components. The parameters are the same as Fig. 1

The finite θ_k destabilization of the odd modes can be understood in a similar way. As shown in Fig. 3, the mode has an odd parity at $\theta_k = 0$, and, hence, cannot be excited by the trapped electrons, due to the bounce averaging. However, as θ_k increases, the eigenmode structure breaks its odd parity, and, thereby, experiences finite trapped-electron instability drive. As θ_k further increases, the eigenmode structure peaks toward $\eta = 0$, where

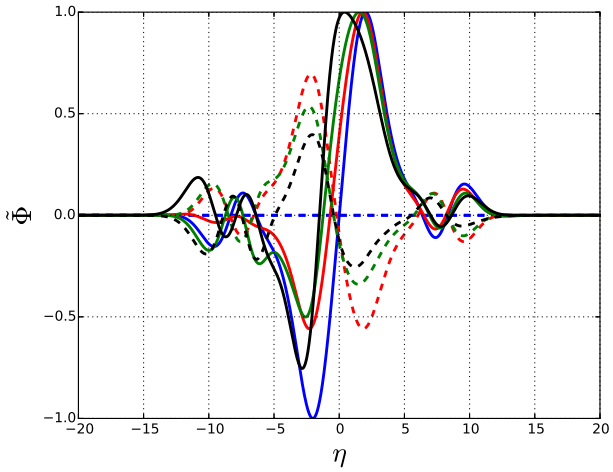

FIG. 3: (Color online) Plots of eigenmode structures of the odd-parity strong toroidicity-induced modes for $\theta_k = 0$ (blue), $\theta_k = 0.5$ (red), $\theta_k = 1.0$ (green) and $\theta_k = 1.63$ (black). The solid (dashed) lines correspond to the real (imaginary) components. The parameters are the same as Fig. 1

the trapped-electron instability drive also peaks. Consequently, as shown in Fig. 1, the odd mode can be significantly destabilized at finite θ_k.

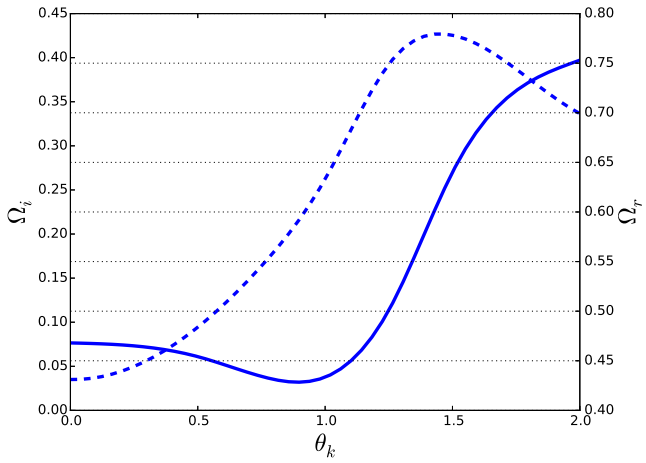

FIG. 4: (Color online) Plots of the eigenfrequencies versus θ_k for the even-parity weak toroidicity-induced eigenmode. The parameters are $\tau = s = \eta_i = 1$, $q = 1.5$, $\epsilon = 0.2$, $\epsilon_n = 0.3$, $k_\theta \rho_i = 0.6$, $\eta_e = 3$. Solid (dashed) line is the real frequency (growth rate).

Similar analyses can be done for the even-parity weak toroidicity-induced mode. Figures 4 and 5 show the plots of, respectively, the eigenfrequencies and eigenmode structures versus θ_k. Note, from Fig. 5, that the even-parity mode peaks away from $\eta = 0$ at $\theta_k = 0$, confirming that it corresponds to a weak toroidicity-induced mode.

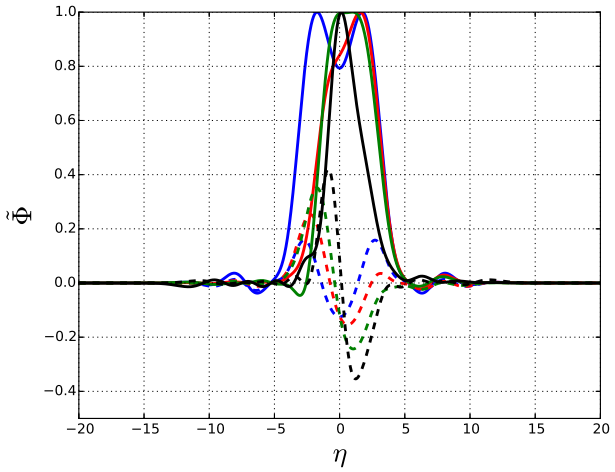

FIG. 5: (Color online) Plots of eigenmode structures of the even-parity weak toroidicity-induced modes for $\theta_k = 0$ (blue), $\theta_k = 0.5$ (red), $\theta_k = 0.75$ (green) adn $\theta_k = 1.50$ (black). The solid (dashed) lines correspond to the real (imaginary) components. The parameters are the same as Fig. 4

Figure 4 indicates that, as θ_k increases, the instability growth rate also increases significantly. Again, the finite θ_k destabilization can be understood, as shown in Fig. 5, in terms of shifting of the eigenmode structure toward $\eta = 0$, where the trapped-electron instability drive is localized. The odd-parity weak toroidicity-induced mode is not shown here as its behavior versus θ_k is similar to that of the odd-parity strong toroidicity-induced mode.

IV. SUMMARY AND DISCUSSIONS

In this study, we have derived an integro-differential eigenmode equation for CTEMs in toroidal plasmas, including the effect of finite radial envelope modulations, i.e., the effect of finite θ_k. We have solved the eigenmode equation numerically for the eigenfrequencies and the corresponding eigenmode structures. Our results indicate that the finite θ_k can modify the linear stability properties both quantitatively and qualitatively. The reasons are the finite θ_k can break the parity symmetry as well as shift the eigenmode peak toward or away from $\eta = 0$, where the bounce-averaged trapped-electron instability drive is concentrated. More specifically, we find that, for the even-parity strong toroidicity-induced mode, which peaks at $\eta = 0$ when $\theta_k = 0$, the peak shifts away from $\eta = 0$ as θ_k increases. On the other hand, for the odd parity mode, which is stable when $\theta_k = 0$, it is destabilized as θ_k increases, due to the peak being shifted toward $\eta = 0$. A similar picture also holds for the even-parity weak toroidicity-induced mode, which has its two peaks located away from $\eta = 0$ when $\theta_k = 0$. As θ_k increases, the peaks merge and shift toward $\eta = 0$, and, thereby, the mode is further destabilized. The odd-parity weak toroidicity-induced mode, meanwhile, has a similar behavior versus θ_k as that of the odd-parity strong toroidicity-induced mode.

Finally, we remark that the present findings of the finite θ_k effects on the linear stability properties have fundamental implications to the nonlinear dynamics of CTEM, since both the CTEM-Zonal flow interactions [17, 18] and the nonlinear mode-mode coupling processes [9, 10, 19] depend crucially on the radial envelope modulations, i.e., the finite θ_k effects. Detailed investigations on these nonlinear processes will be reported in a future publication.

V. ACKNOWLEDGMENTS

One of the authors (H. T. Chen) would like to thank M. Y. Yu and Z. Y. Qiu for useful conversations.

This work is supported by National Magnetic Confinement Fusion Energy Research Program under Grant No.2013GB111004 and the National Science Foundation of China under grant No. 11235009. L. Chen also acknowledges the support of US DoE GRANT.

[1] W. Horton, Rev. Mod. Phys. **71**, 735, (1999).
[2] W. M. Tang, Nucl. Fusion **18**, 1089, (1978).
[3] T. Xie, Y. Z. Zhang, S. M. Mahajan and A. K. Wang, Phys. Plasmas **19**, 072105, (2012).
[4] D. Dickinson, C. M. Roach, J. M. Skipp and H. R. Wilson, Phys. Plasmas **21**, 010702, (2014).
[5] J. C. Adam, W. M. Tang and P. H. Rutherford, Phys. Fluids **19**, 561, (1976).
[6] P. Catto and K. Tang, Phys. Fluids **21**, 1381, (1978).
[7] C. Z. Cheng and L. Chen, Nucl. Fusion **21**, 403, (1981).
[8] J. Q. Dong, S. M. Mahajan and W. Horton, Phys. Plasmas **4**, 755, (1997).
[9] P. L. Similon and P. H. Diamond, Phys. Fluids **27**, 916, (1984).
[10] T. S. Hahm and W. M. Tang, Phys. Fluids B **3**, 989, (1991).
[11] J. W. Connor, R. J. Hastie and J. B. Taylor, Proc. R. Soc. London, Ser. A **365**, 1, (1979).
[12] R. L. Dewar, Plasma Phys. Control. Fusion **39**, 453, (1997).
[13] L. D. Pearlstein and H. L. Berk, Phys. Rev. Lett. **23**, 220, (1969).
[14] L. Chen and C. Z. Cheng, Phys. Fluids **23**, 2242, (1980).
[15] R. J. Hastie, K. W. Hesketh and J. B. Taylor, Nucl. Fusion **19**, 1223, (1979).
[16] H. T. Chen. (to be published).
[17] D. R. Ernst, J. Lang, W. M. Nevins, M. Hoffman, Y. Chen, W. Dorland and S. Parker, Phys. Plasmas **16**,

055906, (2009).
[18] Y. Xiao, I. Holod, W. Zhang, S. Klasky and Z. Lin, Phys. Plasmas **17**, 022302, (2010).
[19] L. Chen, R. L. Berger J. G. Lominadze, M. N. Rosenbluth and R. H. Rutherford, Phys. Rev. Lett. **39**, 754, (1977).